Correction of misalignment introduced aberration in non-null test measurements of free-form surfaces

G. Baer baer@ito.uni-stuttgart.de Institut für Technische Optik, University of Stuttgart, Pfaffenwaldring 9, 70569 Stuttgart, Germany

J. Schindler Institut für Technische Optik, University of Stuttgart, Pfaffenwaldring 9, 70569 Stuttgart, Germany

C. Pruss Institut für Technische Optik, University of Stuttgart, Pfaffenwaldring 9, 70569 Stuttgart, Germany

W. Osten Institut für Technische Optik, University of Stuttgart, Pfaffenwaldring 9, 70569 Stuttgart, Germany

In interferometric testing of surfaces a major task is to avoid the introduction of aberrations due to misalignment of the surface under test. An automated method for the positioning of aspheric and free-form surfaces in a non-null test interferometer, as well as a method for the distinction between alignment introduced aberrations and surface errors is presented. A combination of both methods allows for a fully automated alignment with low requirements to the accuracy of the positioning stage. Further, the misalignment introduced uncertainties to the measurement are estimated. Simulation results as well as experimental results showing the feasibility of the method are presented.
[DOI: http://dx.doi.org/10.2971/jeos.2013.13074]

Keywords: Aspheres, free-forms, alignment, non-null test, interferometry

1 INTRODUCTION

Aspheric surfaces have become the solution of choice in modern high-end optics [1, 2]. The advantage of aspherical elements, compared to classical spherical or planar optics, is the highly increased degree of freedom for the optics design. Therefore the use of aspherical elements allows the reduction of aberrations, by simultaneously reducing the required amount of elements needed to fulfill a given design target. This leads to more compact and lightweight systems with higher optical performance. If the rotational symmetry of the aspheric surface is broken even more degrees of freedom are available for the optics design. Such so called free-form surfaces allow the construction of even more sophisticated optical systems. Possible applications are systems, where the optical elements are no longer aligned along a straight line, but where the optical axis is folded. This method allows the construction of more compact systems that are less vulnerable to mechanical stress or vibrations. Further, for some wavelengths - for example in the EUV range - no refracting materials with tolerable absorption are available. Here the construction of off-axis mirror optics is the solution of choice which can be realized by the use of free-form surfaces. The technique for the fabrication of aspheric and free-form surfaces has made a major progress in the last years. Methods like ion beam etching, magneto rheological finishing (MRF) or diamond turning allow the flexible manufacturing of aspheric and free-form surfaces. However, since the measurement is needed for the control of these processes, a surface can only be fabricated as well as it can be measured.

Therefore metrology is as important as the fabrication technique itself. The challenge when measuring a surface that deviates from the spherical form interferometrically is, that the rays do no longer hit the surface perpendicularly. This violation of the null-test condition can lead to high fringe density that cannot be evaluated if the Nyquist criterion is broken. If the slope deviation is even higher the light might get vignetted completely. Further, since the rays take different paths through the interferometer on their way back, retrace errors are introduced to the measurement [3, 4]. One solution to overcome these problems is to restore the null-test condition by compensation optics that adapts the wavefront to the shape of the surface under test. Such optical elements can be realized as computer generated holograms (CGH), which is state of the art in high end asphere and free-form metrology [5, 6]. The drawback here is, that for every design shape a matching CGH has to be fabricated. Another approach is to restore the null-test condition sequentially for small parts of the surface. Known realizations of this approach is the scanning Fizeau interferometer [7] or stitching interferometry [8, 9]. The drawback of all scanning and stitching methods is the long measurement time, since the surface under test (SUT) has to be moved during the measurement.

The interferometer this work is based on, uses an extended array of point sources that, after being collimated, form a variety of wavefronts with different amounts of tilt [10]. The tilt of the wavefronts is used to locally compensate the deviation of the surface from the spherical form. Because of the tilted waves we call the method Tilted-Wave-Interferometry (TWI). Since the application of the wavefronts to the surface is highly par-

Received August 23, 2013; revised ms. received September 30, 2013; published November 03, 2013 ISSN 1990-2573

allelized a short measurement time of only about 30 seconds can be achieved. Further, it is highly flexible and has a high dynamic range up to 10° slope deviation from the spherical form, without the need of costly compensation optics.

As in every interferometric measurements, the alignment of the surface under test plays an important role. If the surface is misaligned, additional aberrations are introduced to the measurement. In case of spherical and planar surfaces it is possible to distinguish between the alignment introduced aberrations and aberrations of the surface itself. However, for aspheric surfaces this task is not trivial any more [11]–[13]. Furthermore, through the misalignment, additional retrace errors are introduced. Therefore it is inevitable to align the surface as good as possible. In the case of aspherical surfaces we already demonstrated, that the alignment in three translational dimensions can be automated very well [14]. Here remaining tilt is compensated by decentering of the SUT. In the general case of free-form surfaces, that do not show any rotational symmetry this method cannot be applied any more. The alignment of the surface has to be performed in six degrees of freedom (DOF) and no symmetry condition can be used for the alignment. In this work we present a method for the alignment of free-form surfaces as well as a method to separate the alignment introduced aberrations and the alignment introduces retrace errors from the measurement result of aspheric and free-form surfaces. By combining the algorithms for the alignment and the correction of the misalignment introduced aberrations the whole measurement process can be easily automated. Further the requirements to the positioning stage can be reduced by several orders of magnitude compared to null-test measurements.

2 THE TILTED-WAVE-INTERFEROMETER

2.1 Setup

In Figure 1 the basic setup of the Tilted-Wave-Interferometer is shown. A coherent laser source L is divided into a test and a reference wave by a polarizing beam splitter PBS. The light in the test wave is used to illuminate a micro lens array that is followed by a pinhole array. These two parts serve as an array of point sources for the test wavefronts. The spherical wavefront from each point source is, after passing the beam splitter BS, collimated by C1 resulting in a set of plane wavefronts with different amounts of tilt [10], [15, 16]. The tilted wavefronts are transformed to spherical wavefronts by the transmission sphere TS to compensate the basic spherical form of the SUT. In the case of surfaces with a best fit sphere of infinite radius no transmission sphere is needed. After being reflected by the SUT the wavefronts propagate back to the beam splitter where they are reflected to the camera arm of the interferometer. In the Fourier plane an aperture stop is located, to block all light that would generate fringes with a density that violates the Nyquist criterion. After the aperture the light passes an imaging optics L1 and interferes with the reference wavefront on the camera C. The distance between the sources in the array is chosen to cover the whole SUT without gaps and a slight overlap. To avoid interference between neighboring sources the measurement is divided into four steps, with only every

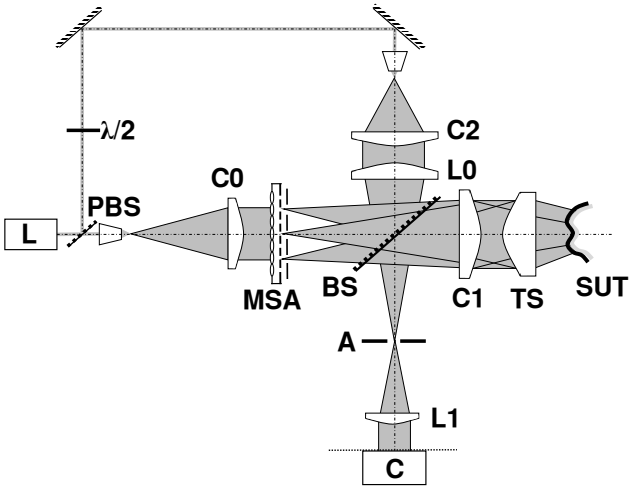

FIG. 1 Schematic setup of the Tilted-Wave-Interferometer.

fourth source enabled in each step. The switching between the sources is realized by a simple aperture array that is moved in front of the micro lenses and blocks every second source in each row and column. The main difference of this approach to the scanning type interferometers described above is that the acquisition of the data is highly parallelized since all the test wavefronts are applied to the surface in only four steps. Further, the SUT does not have to be moved during the measurement process. Both these advantages lead to a very short measurement time of about half a minute.

2.2 Calibration and measurement

Like with all non-null test methods the calibration of the device is an important task [3]. For the calibration a black-box model of the interferometer is used. The model consists of two black boxes, one describing the wavefront aberrations of the test wavefronts coming from the sources, the second black-box describes the interferometer from the test space to the camera. For the calibration a perturbation method is used [17]. With the calibrated black-boxes it is possible to perform ray tracing calculations with arbitrary objects in the test space. This allows to not only calculate the optical path length for each ray on the camera, but also the exact intersection point and angle with the SUT, without having to know the specific aberrations of the optical elements in the device. The measurement evaluation is performed in two steps. The first step is the calculation of the basic surface shape which is represented as polynomial. The second step it the evaluation of higher spacial frequencies that are not covered by the polynomial [18]. As final result the surface reconstruction including the basic shape, but also mid and high spatial frequencies is obtained.

3 AUTOMATED ALIGNMENT OF FREE-FORM SURFACES

In the case of a rotationally symmetric aspheres we already demonstrated, that the alignment in three dimensions can be performed using an iterative algorithm [14]. The reproducibility of the alignment by this approach is about 1 µm in space. In the general case of a free-form surfaces, the alignment has to be performed in up to six degrees of freedom. Free-form

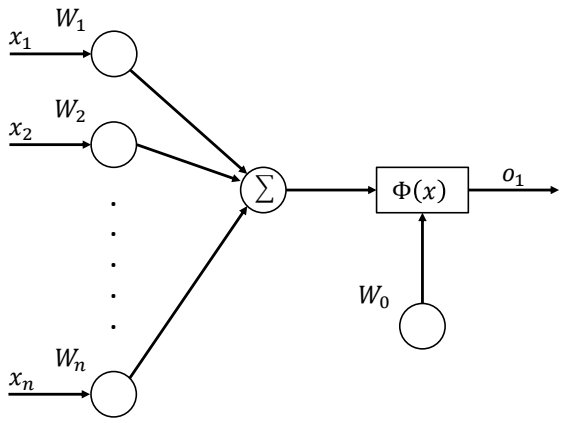

FIG. 2 Schematic setup of a single neuron with input x_i, weight W_i, transfer function ϕ and output o_1.

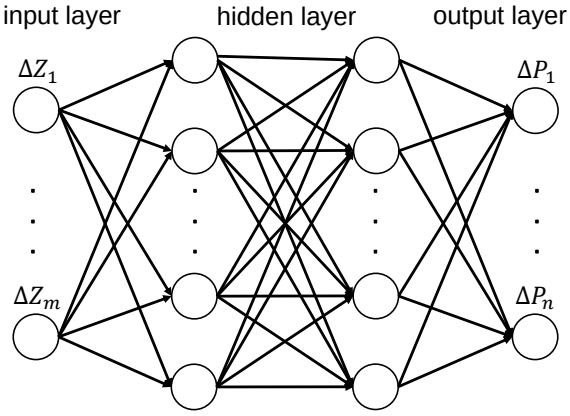

FIG. 3 Schematic setup of a neural network with input layer, two hidden layers and output layer. Neurons are illustrated as circles and the connections between them as arrows.

surfaces exist in a variety of shapes and the description of the surface is not standardized as it is the case with aspheric surfaces. This makes it difficult to find an analytic solution for the alignment problem, since for every new design shape a new transfer function has to be calculated and the algorithm has to deal with many different surface representations from point clouds to different polynomials or splines. The solution we present here uses artificial neural networks [19]. Such networks consist of simple neurons as shown in Figure 2. The calculation of each neuron works as follows: Each input value x_i of the neuron is multiplied with the corresponding weight W_i (circles). All the weighted inputs are summed up and the result serves as input for the transfer function ϕ

$$o_1 = \phi(\sum_{i=1}^{n} x_i W_i, W_0) \tag{1}$$

The output of the neuron o_1 is calculated by the transfer function ϕ which is implemented as a sigmoid function where W_0 defines the threshold value.

A neural net consists of several neurons that are organized in layers as shown in Figure 3. The first layer is defined by the input data. The output of each neuron in a layer is fed to one input of each neuron in the following layer. The output of the last layer is the result calculated by the neural net. By training the net with a set of given samples it learns to compute a given task by adapting the weights W_i of the neurons [20]. The advantage of this approach is, that the solution works independent from the surface description and surface shape. Another advantage is, that neural nets are able to adapt to strong nonlinear functions and allow a global optimization in contrast to gradient based approaches where only local minimums are found. In the first step the surface is coarsely aligned until fringes can be seen on the camera. The coarse alignment is performed manually or by knowledge of the surface geometry relatively to the mounting mechanics. Here an accuracy of 0.1 mm in space is sufficient. To detect the misalignment an interferometric phase shifting measurement of the surface serves as input. In Figure 4 a simulated modulo 2π phase map of a free-form surface with a basic astigmatic shape is shown. The surface in this example is described by 136 Zernike coefficients. The shape of the patches depends on the basic shape of the SUT and the position in the test area. In regions with low fringe density circular areas are defined on the camera and Zernike polynomials [21] of order j are fitted to the evaluated phase in each circular subaperture. In most cases a polynomial order of 15 is sufficient.

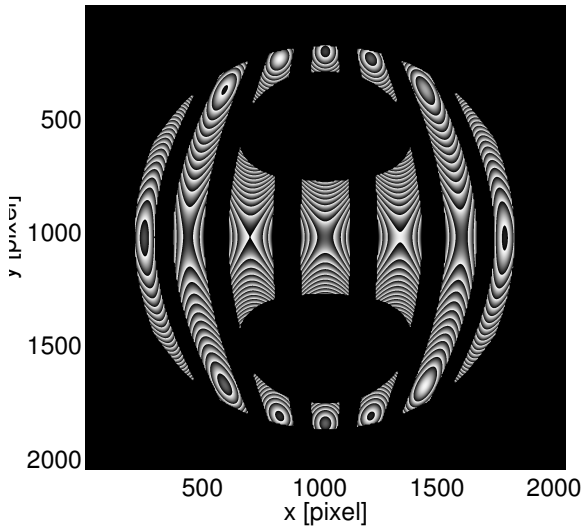

FIG. 4 Simulated modulo 2π phase map of a free-form surface (the wavelength is increased for better visualization).

Using the black-boxes from the calibration and the nominal shape of the SUT the phase map in each circular test area is calculated for a perfect aligned surface. With knowledge of the accuracy of the coarse alignment pseudo random positions that lie within the tolerances of the positioning accuracy are defined and the phase maps in the test areas are calculated for each position. Now we fit Zernike polynomials of the order j to the test areas of the perfect aligned as well as the misaligned surfaces. With the difference of the Zernike coefficients

$$\Delta \mathbf{Z} = \mathbf{Z}(P_i) - \mathbf{Z}(P_0) \tag{2}$$

where $\mathbf{Z}(P_i)$ is a vector of Zernike coefficients at a random position and $\mathbf{Z}(P_0)$ are the coefficients of the perfectly aligned surface and the corresponding random position the neural network is trained. The alignment is performed iteratively. In each step a interferometric measurement of the surface is acquired and Zernike polynomials are fitted to the test areas. With the coefficients of the fit minus the coefficients of the perfect aligned surface as input, the neural network computes the corrected position. In Figure 5 simulation results for the alignment of a free-form surface is plotted for three different start

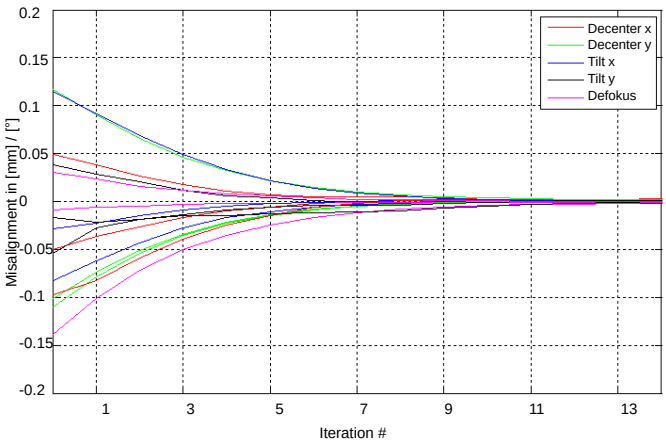

FIG. 5 Convergence of alignment process: Simulation result for three different start positions.

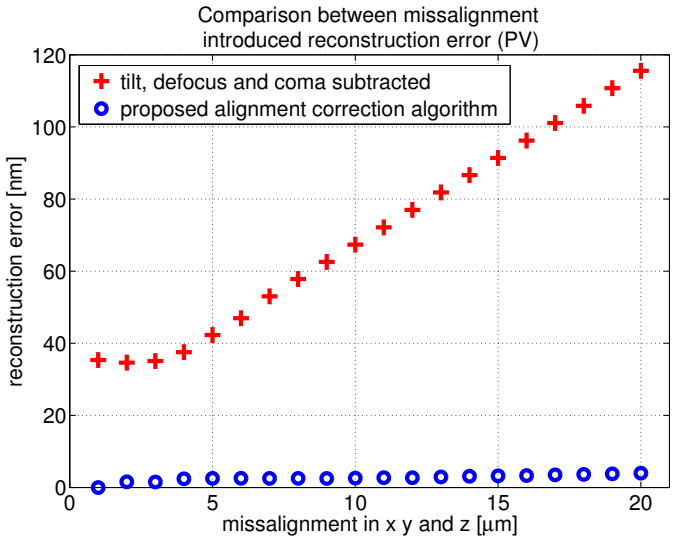

FIG. 6 Simulated reconstruction error introduced to measurement by misalignment. With the proposed algorithm the error stays below 5 nm (o symbol) whereas the error increases with misalignment if simply the alignment introduced aberrations (tilt, defocus, coma) are subtracted. (+ symbol).

positions. It was assumed that the surfaces shape was known. As can be seen the convergence is fast with a reproducibility of about 2 µm in space after 12 iterations.

4 CORRECTION OF ALIGNMENT ERRORS

The TWI measures the misaligned surface as is, including alignment errors. However, since the whole test space is calibrated, all retrace errors are taken into account correctly. This means, that the measurement result is only translated and rotated in space, but there is no error introduced to the surface reconstruction, that would change the surface shape. Therefore, to reconstruct the measurement without alignment errors, the result has to be rotated and translated back to its nominal position. This is achieved by a variation method. The first step of the algorithm is to fit the nominal surface with a Zernike polynomial of order v. The measurement is available as a point cloud $\mathbf{D} = [\mathbf{x}, \mathbf{y}, \mathbf{z}]$ with a x, y and z value for each point. In the second step of the algorithm this point cloud is translated by a small amount ϵ in x,y and z and rotated around the three axis (α, β, γ). Each of these translated or rotated point clouds is then fitted by a Zernike polynomial of order v and the result of the Zernike fit for each direction minus the Zernike coefficients of the initial point cloud forms a column of the variation matrix.

$$A = \begin{pmatrix} \frac{\partial Z_1}{\partial x} & \frac{\partial Z_1}{\partial y} & \frac{\partial Z_1}{\partial z} & \frac{\partial Z_1}{\partial \alpha} & \frac{\partial Z_1}{\partial \beta} & \frac{\partial Z_1}{\partial \gamma} \\ \vdots & \vdots & \vdots & \vdots & \vdots & \vdots \\ \frac{\partial Z_v}{\partial x} & \frac{\partial Z_v}{\partial y} & \frac{\partial Z_v}{\partial z} & \frac{\partial Z_v}{\partial \alpha} & \frac{\partial Z_v}{\partial \beta} & \frac{\partial Z_v}{\partial \gamma} \end{pmatrix} \tag{3}$$

with

$$\frac{\partial Z_1}{\partial x} = \frac{Z_1([\mathbf{x}, \mathbf{y}, \mathbf{z}] - Z_1[\mathbf{x} + \epsilon, \mathbf{y}, \mathbf{z}])}{\epsilon} \tag{4}$$

If the nominal surface geometry features some sort of symmetry, the corresponding degree of freedom has to be taken out of the calculation. For example in case of a rotationally symmetric, aspheric surface the rotation about the optical axis z has no effect on the result and therefore the 6_{th} column is obsolete. With $\Delta\mathbf{Z} = \mathbf{Z}_{nom} - \mathbf{Z}_{measure}$ and the matrix $\mathbf{A}$ the correction vector $\mathbf{b}$ can be calculated by solving the least square problem using well known regularization algorithms.

$$||\mathbf{Ac} - \Delta\mathbf{Z}||^2 \tag{5}$$

As result we obtain the correction term $\mathbf{c}$. The measured point cloud is now translated and rotated by the values in $\mathbf{c}$. The calculation is iterated until a convergence is reached. To reduce numerical noise and since the rotations in three dimensions are not orthogonal in every iteration n the correction values in $\mathbf{c}$ are summed up over the previous iterations and the original point cloud is rotated.

$$\mathbf{c} = \sum_{i=1}^{n} \mathbf{c}_i \tag{6}$$

As final result the corrected surface without alignment errors is obtained. Further, the correction term $\mathbf{c}$ of the last iteration contains the information about the misalignment of the surface during the measurement. This information can be used to reference the surface orientation and position.

5 ESTIMATION OF UNCERTAINTIES

To estimate the uncertainties introduced by misalignment of the SUT and to prove the feasibility of the algorithm, a simulation was performed. For the simulation an aspheric surface with 8° deviation of its best fit sphere was misaligned and the surface was reconstructed using the TWI algorithms. As reference a perfect aligned surface was reconstructed. In Figure 6 the alignment introduced reconstruction error is plotted in dependence of the misalignment. As comparison the alignment introduced error when subtracting the adjustment terms (tilt, defocus and first order coma) is plotted (+ symbol) .The result obtained by the proposed algorithm (o symbol) shows, that even if the surface is misaligned by 20 µm in x, y and z the

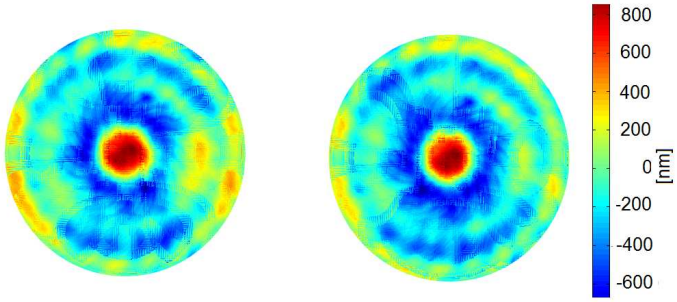

FIG. 7 Reproducibility measurement of an aspheric surface. On the left with surface perfect aligned, on the right with 20 µm misalignment.

misalignment introduced error stays below 5 nm, whereas the error when subtracting alignment terms is over 100 nm for the same amount of misalignment. Even for the perfect aligned system the algorithm performs better than the subtraction of alignment terms. This is because the real surface shape may contain aberrations like coma, and therefore an error is introduced when subtracting them.

6 EXPERIMENTAL RESULTS

To test the algorithm with real measurement data, an aspheric surface was measured in two positions. The first position with the surface aligned as well as possible, the second position with an intentional misalignment of 20 µm in x direction. As can be seen in Figure 7 the reproducibility of the measurement is good and remains within the reproducibility of the current lab setup.

7 CONCLUSION

We could show that the alignment of the SUT can be automated very well not only in case of aspheric, but also the more general case of free-form surfaces. With the presented algorithm it is further possible to distinguish between misalignment introduced aberrations including adjustment terms like tilt, defocus and coma, but also retrace errors and the surface shape. A combination of both methods allows to fully automate the alignment process by simultaneously lowering the requirements to the positioning stage.

8 ACKNOWLEDGEMENTS

The EMRP is jointly funded by the EMRP participating countries within EURAMET and the European Union. We further thank the Baden-Württemberg Stiftung for financing parts of this work.

References

[1] B. Braunecker, R. Hentschel, and H. J. Tiziani (eds.), *Advanced Optics Using Aspherical Elements* (SPIE Press, Bellingham, 2008).

[2] G. Schulz, "Aspheric Surfaces," in *Progress in Optics, Vol. XXV*, E. Wolf, ed., 349–415 (Elsevier Science Publishing, Amsterdam, 1988).

[3] C. J. Evans, and J. B. Bryan, "Compensation for errors introduced by nonzero fringe sensities in phase-measuring interferometers," CIRP Ann-Manuf. Techn. **42**, 577–580 (1993).

[4] A. E. Lowman, and J. E. Greivenkamp, "Interferometer errors due to the presence of fringes," Appl. Optics **35**, 6826–6828 (1996).

[5] D. Malacara, K. Creath, J. Schmit, and C. Wyant, "Testing of Aspheric Wavefronts and Surfaces," in *Optical Shop Testing*, D. Malacara, ed., (3rd ed, John Wiley & Sons, Hoboken, 2007).

[6] T. Yatagai, and H. Saito, "Interferometric testing with computer-generated holograms: aberration balancing method and error analysis," Appl. Optics **17**, 558–565 (1978).

[7] M. F. Kuechel, "Absolute measurement of rotationally symmetric aspheric surfaces," in *Proceedings to Optical Fabrication and Testing (OFT)*, 1–3 (OSA, Rochester, 2006).

[8] P. Murphy, G. Forbes, J. Fleig, P. Dumas, and M. Tricard, "Stitching interferometry: a flexible solution for surface metrology," Opt. Photonics News **14**, 38–43 (2003).

[9] M. Tricard, "Subapertur-Stitching-Interferometrie: Messtechnik für die AsphärenPräzisionsfertigung," Opt. Photonics News **6**, 38–41 (2008) in German.

[10] E. Garbusi, C. Pruss, and W. Osten, "Interferometer for precise and exible asphere testing," Opt. Lett. **33**, 2973–2975 (2008).

[11] G. C. Dente, "Separating misalignment from misfigure in interferograms on off-axis aspheres," in *Proceedings to SPIE Precision Surface Metrology*, 187–193 (SPIE, San Diego, 1983).

[12] E. W. Young, and G. C. Dente, "The effects of rigid body motion in interferometric tests of large-aperture, off-axis, aspheric optics," in *Proceedings to SPIE Southwest Conference on Optics*, 59–68 (SPIE, Albuquerque, 1985).

[13] B. Dörband, and H. J. Tiziani, "Testing aspheric surfaces with computer-generated holograms: analysis of adjustment and shape errors," Appl. Optics **24**, 2604–2611 (1985).

[14] G. Baer, E. Garbusi, W. Lyda, and W. Osten, "Automated surface positioning for a non-null test interferometer," Opt. Eng. **49**, 095602-095602-12 (2010).

[15] J. Liesner, E. Garbusi, C. Pruss, and W. Osten, "Verfahren und Messvorrichtung zur Vermessung einer optisch glatten Oberfläche" Patent DE 10 2006 057 606 A1 (2006) in German.

[16] J. Liesner, *Zum Einsatz räumlicher Lichtmodulatoren in der interferometrischen Wellenfrontmesstechnik* (Ph.D. thesis, Universität Stuttgart, 2006) in German.

[17] E. Garbusi, and W. Osten, "Perturbation methods in optics: application to the interferometric measurement of surfaces," J. Opt. Soc. Am. A **26**, 2538–2549 (2009).

[18] G. Baer, J. Schindler, J. Siepmann, C. Pruss, W. Osten, and M. Schulz, "Measurement of aspheres and free-form surfaces in a non-null test interferometer: reconstruction of high-frequency errors," in *Proceedings to SPIE 8788, Optical Measurement Systems for Industrial Inspection VIII*, 10.1117/12.2021518 (SPIE, Munich, 2013).

[19] K. Hornik, M. Stinchcombe, and H. White, "Multilayer feedforward networks are universal approximators," Neural Networks **2**, 359–366 (1989).

[20] M. T. Hagan, and M. B. Menhaj, "Training Feedforward Networks with the Marquardt Algorithm," IEEE T. Neural Networ. **5**, 989–993 (1994).

[21] J. Y. Wang, and D. E. Silva, "Wave-front interpretation with Zernike polynomials," Appl. Optics **19**, 1510–1518 (1980).